

UC Santa Barbara

UC Santa Barbara Previously Published Works

Title

Electrochemical control of specific adhesion between amine-functionalized polymers and noble metal electrode interfaces

Permalink

<https://escholarship.org/uc/item/6js04071>

Journal

Materials and Corrosion, 65(4)

ISSN

0043-2822

Authors

Donaldson, SH
Utzig, T
Gebbie, MA
[et al.](#)

Publication Date

2014-04-01

DOI

10.1002/maco.201307581

Copyright Information

This work is made available under the terms of a Creative Commons Attribution-NonCommercial License, available at <https://creativecommons.org/licenses/by-nc/4.0/>

Peer reviewed

Electrochemical control of specific adhesion between amine-functionalized polymers and noble metal electrode interfaces

Dedicated to Professor Dr. Martin Stratmann on the occasion of his 60th birthday.

S. H. Donaldson Jr., T. Utzig, M. A. Gebbie, S. Raman,
B. R. Shrestha, J. N. Israelachvili and M. Valtiner*

Polymers are widely utilized as protective coatings to prevent metal surfaces from wear, corrosion, or bio-fouling. Yet, stability and adhesive properties of polymer to metal bondings are not fully understood at the molecular level. Here, we measured the interaction forces between a gold electrode surface and amine-functionalized polymers (PEG) using a novel electrochemical surface forces apparatus. We examined the potential dependence of specific amine–gold interactions and measured that the binding strength of amine–gold bonds can range from 0.5 to 40 $k_B T$ per binding site, depending on the applied electrochemical potential. Notably, this interaction exhibits a pronounced minimum around the potential of zero charge, where the polymer–gold adhesion is dominated by non-specific interactions between the polymer backbone and electrode surface, consistent with the adhesion of PEG polymers with gold surfaces in the absence of amine functionalization. Further, repulsive hydration interactions were observed to be stronger for amine-terminated PEG compared to non-functionalized PEG, due to increased hydration and presence of counterions in the case of amine-terminated PEG. Our results provide molecular-scale insight into design and optimization of polymer coatings for numerous applications requiring strong, specific binding interactions between polymers and metals (or their native oxides), for example passivating layers in biomedical implants and electronic devices.

1 Introduction

Interaction forces at soft matter/metal interfaces determine the structures, functionalities, and stabilities of materials in a wide range of technological and medical applications. For example, a

S. H. Donaldson Jr., J. N. Israelachvili
Department of Chemical Engineering, University of California, Santa Barbara, CA 93106-5080, (USA)

T. Utzig, S. Raman, B. R. Shrestha, M. Valtiner
Interface Chemistry and Surface Engineering, Max-Planck-Institut für Eisenforschung GmbH, D-40237 Düsseldorf, (Germany),
E-mail: valtiner@mpie.de

M. A. Gebbie, J. N. Israelachvili
Materials Department, University of California, Santa Barbara, CA 93116, (USA)

detailed understanding of the complex interactions of cell membranes and lipid vesicles with metal nanoparticles is critical to establish knowledge based engineering and design of nano-materials as safe and efficient drug carriers [1–3]. Moreover, interactions of biological materials and fluids with metal and/or metal oxide surfaces can strongly influence (i.e., typically accelerate) the corrosion and/or tribo-corrosion rates of implanted materials such as hip-replacements or stents used for the relief of artery blockages [4]. Further, the adhesion between a polymer or organic coating and an engineering-metal surface (which is typically oxide covered) is crucial to achieve desired properties such as increased wear protection [5], electrical insulation [6] or corrosion protection [7]. In particular, organic-based paints have been widely used as an effective and cheap protective coating for steel and various other structural and functional materials, which are prone to corrosion. All of the above applications share the common theme that the initiations

and rates of corrosive reactions are critically influenced, and may be controlled and mediated, by the interactions of soft matter (whether it is polymers or biological materials) with metallic materials.

Stratmann, to whom this article is dedicated, is well recognized for his pioneering studies of local electrochemical potentials and reactions at interfaces comprised of organic coatings in contact with metal and metal-oxide surfaces at the micro- and nano-scale. An intact polymer coating can slow down corrosion rates even for bare iron surfaces by orders of magnitude [8–11]. These remarkable protective properties of organic coatings at ambient conditions are not simply a result of the increased barrier properties of the coating for water and oxygen, the two main reactants involved in corrosive reactions. In contrast, diffusion rates of water and oxygen through polymer coatings are typically fast enough to potentially give rise to high corrosion rates. Yet, the very low solubility of ions in polymer matrices [8] can lead to both low conductivities and extended electrical double layers with large effective Debye lengths at metal/polymer interfaces. Low ion mobilities and concentrations can prevent the short-circuiting of local cathodes and anodes, leading to strongly increased activation barriers for, and hence much decreased rates of, interfacial corrosion reactions.

Remarkably, if a protective polymer coating is damaged on a molecular scale, for example only a small fraction of the polymer–metal bonds break, water layers at the interface may be formed almost instantly [8] and corrosive reactions can consequently be accelerated. With the invention of the scanning Kelvin probe [11], which can measure local electrochemical potentials underneath a coating, it was shown that a significant anodic metal dissolution takes place at a defect area with delaminated polymer [8]. This, in turn, leads to an increasing concentration of charge carriers in the interfacial water layer at a defect interface between a polymer and a metal, and corrosive reactions can be initiated with a nearby local cathodic area. It was shown that local cathodes are typically located at the intact metal/polymer interface [8]. At the local cathode, oxygen reduction proceeds at low electrochemical potentials. This leads to both (1) a strong alkaline pH-shift, and negative charge that is, hydroxide accumulation (which can trigger the migration of metal ions toward an intact polymer metal interface, initiating a local corrosion element [12,13]), and (2) formation of aggressive corrosion products like H_2O_2 or radicals. Such aggressive species can attack metal/polymer bonds to initiate further and progressive delamination of the protective coating, which accelerates the subsequent disintegration of the coated material.

However, it has also been shown that the molecular structure of a polymer can strongly influence interfacial electrochemical processes [14,15], and the development of smart coatings, with integrated adaptive mechanisms [16] or specific functional groups [17], may effectively inhibit or slow down the corrosion of various materials. In spite of the importance of this field for a wide range of applications, the interactions and adhesion of polymer molecules with electrochemically active interfaces are still poorly understood at the molecular level. Here, we discuss recent experimental advances made using our newly designed electrochemical surface forces apparatus (EC-SFA)

[18–21], which allows the direct quantification of interaction forces at electrochemically active metal surfaces. In particular, we discuss how we can uniquely unravel and quantify molecular-scale effects of the polymer-backbone and polymer-functionalization on interaction forces, and resultant adhesion, of polymers with metallic model surfaces over a wide range of applied electrochemical potentials. Our results and approach provide a rationale for designing functional polymers for both the prevention of corrosion as well as for smart adaptive coatings for biomaterials applications.

2 Methods and materials

2.1 EC-SFA and interaction force measurements

All force measurements were performed in 5 mM (pH 2.3) or 1 mM (pH 3.0) HNO_3 solution (as noted) using an SFA-2000 setup obtained from SurForce LLC (Santa Barbara, USA) with the interacting surfaces either in a crossed-cylinder or a flat-sphere geometry, which are both equivalent and with a nominal radius of curvature $R = 2$ cm. The electrochemical three-electrode attachment for the SFA 2000 consists of the gold working electrodes (WE), a platinum counter electrode (CE) as well an Ag|AgCl (3 M KCl) reference electrode, to which the external potential, U , is referenced during the experiment. The externally applied potential is shifted towards the potential of zero charge, which is at about +140 mV with respect to the Ag|AgCl electrode used as our experimental reference [22]. Measurements were done at 23 °C and only normal forces are reported in this study. For the measurement of the distance and the actual surface geometry (experimental radius, R), white light multiple beam interferometry was employed, which produces so called fringes of equal chromatic order (FECO). For details, the reader is referred to our earlier work [18–21,23–25].

2.2 Details of the experimental system

As shown in Fig. 1a, we applied an electrochemical potential U to a gold electrode surface and simultaneously measured the ensuing force–distance profiles between the electrified gold electrode and lipid bilayers with short-chain and end-functionalized poly-ethylene-glycol (PEG) molecules extending from the bilayer as displayed in the schematic in Fig. 1b. We used two different head-group modifications for the PEG: First, CH_3 terminated PEG_{45} molecules present a model system in which the backbone is terminated by a chemical functionality similar to the backbone chemistry. As second modification we introduce NH_3^+ functionalities as head-group. The NH_3^+ functionality is positively charged at the acidic experimental conditions. In the schematic, the thickness of the lipid bilayer T_{BL} , which is typically 6–7.5 nm for hydrated bilayers [25], is indicated. Throughout the manuscript, we refer the applied electrochemical potentials with respect to the potential of zero charge, U_{PZC} , where the effective surface charge density of the gold surface is zero. The zero distance, D_0 , where $D = 0$ is defined as the distance between gold and mica in dry nitrogen atmosphere, with no applied electrochemical potential.

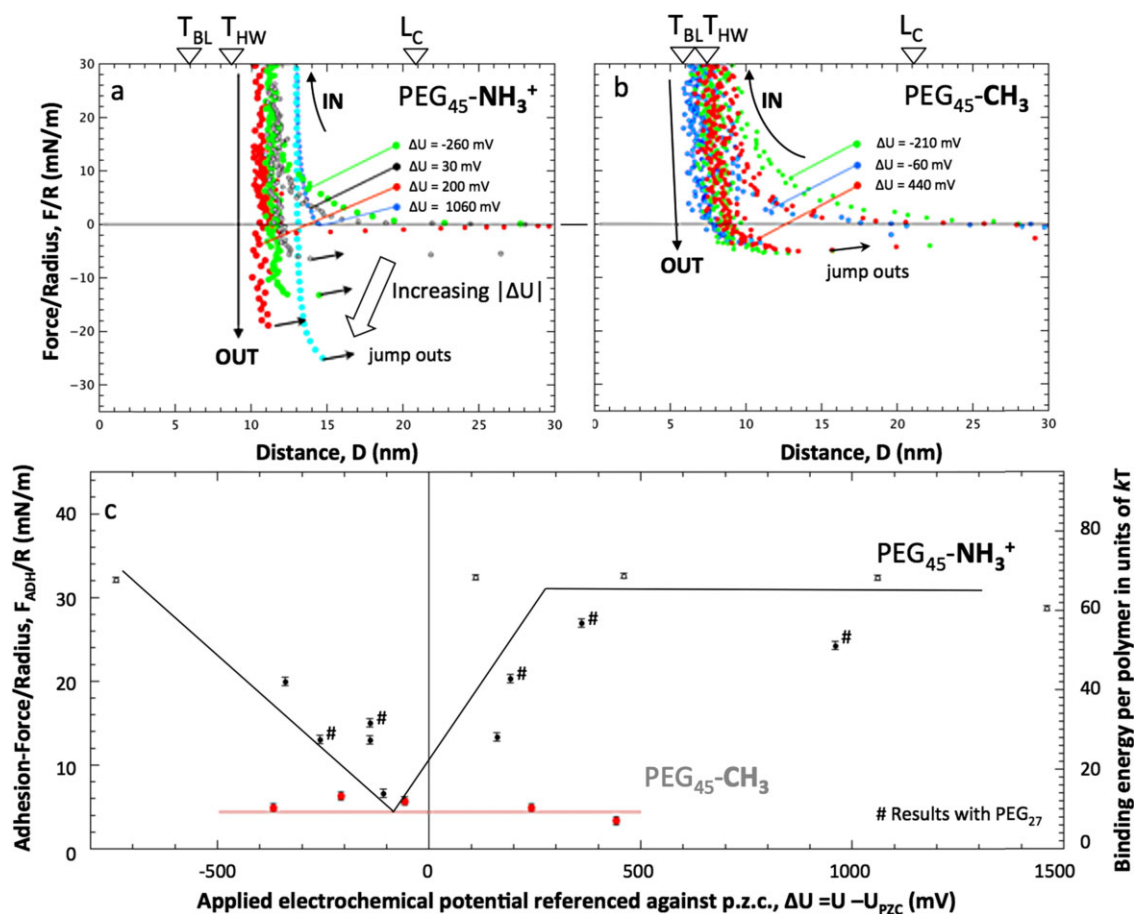


Figure 2. (a) Forces between an end-grafted and end-functionalized $\text{PEG}_{45}\text{-NH}_2$ surface and an electrified gold surface in 5 mM aqueous HNO_3 . (b) Forces between an end-grafted and end-functionalized $\text{PEG}_{45}\text{-CH}_3$ surface and an electrified gold surface in 5 mM aqueous HNO_3 . Both plots (a) and (b) show representative force–distance profiles measured during approach (IN) and separation (OUT) at varying applied electrochemical potentials $\Delta U = U - U_{PZC}$ as indicated. (c) Measured adhesive pull-off force $-F_{ADH}$ (normalized by the radius of curvature, R) between the PEG-functionalized bilayer surface and gold electrode surfaces as a function of the electrochemically applied potential ΔU . Measurements plotted here were recorded either at UC-Santa Barbara or at the MPIE, and results from both labs exhibit excellent agreement and demonstrate the presence of a strong specific binding between gold and $-\text{NH}_3^+$ functionalities. The indicated lines are not a fit to any theory and only added as guidelines

lipids with different head-group functionalities (Fig. 1b). Details of the EC-SFA method have been explained in our previous work [18–21,23–25] and are briefly summarized in Fig. 1a and in the experimental section.

Figure 1b shows a detailed schematic of the interfaces studied in this work. For the measurements presented here, we used a mono-disperse chain length of 45 units for the PEG polymers facing a molecularly smooth gold surface, which was prepared by a template stripping method [20,26]. Furthermore, both an amine terminal group ($-\text{NH}_3^+$, positively charged at the experimental pH 2.3) as well as a methyl terminal group ($-\text{CH}_3$), meaning one additional methyl unit in the 45 unit the PEG-backbone, were studied separately. Through variation of the electrochemical potential, U , the surface potentials $\Phi_{Au}(U)$ and the related surface charge densities $\sigma_{Au}(U)$ of the gold electrode surface were controlled, and hence the electric double layer structure at the gold electrode surface can be varied in situ. Moreover, the chemical nature of the metal surface can be varied by applying positive electrochemical potentials that are more positive than the gold oxidation potential in the HNO_3 solution

$U_{OX} = +900$ mV (vs. U_{PZC}), leading to the growth of a few Å to nm thin gold oxide film at the surface [20,29]. This allows us to directly study the effect of varying electrochemical potentials and electrochemically induced surface reactions (such as surface oxidation (i.e., corrosion), on the interaction forces between gold electrodes and PEG-functionalized lipid bilayer surfaces. In our experiments, the surface density of the PEG-functionalized lipids, and hence the average distance between the end-grafted PEG-functionalized lipids molecules, was fixed at 0.7–0.9% for the NH_3^+ - and CH_3 -terminated PEG-functionalized lipids respectively. This concentration results in a so-called “mushroom” distribution of the polymers at the surface, in which the polymers do not laterally interact with each other, allowing a direct quantification of interaction forces based on fixed number densities of polymers. The contour length L_C of the PEG molecules, that is, the length at full extension, is 16.8 nm, assuming a typical length of an individual segment of 0.365 nm [25]. This defines the maximum distance that the PEG molecules can explore, L_C . The average statistical radius of the solvated PEG molecules in a good solvent is called the Flory

radius [23] $R_F = l \cdot n^{\frac{1}{3}}$ where $l = 0.365$ nm is the length of one monomer segment and $n = 45$ is the number of polymer segments. For the PEG polymers used here, $R_F = 3.6$ nm. In a theta solvent, which assumes no monomer–monomer interactions, the radius of gyration, R_G becomes the relevant statistical size, where the radius of gyration [23] is defined as $R_G = \frac{l\sqrt{n}}{\sqrt{6}}$. For the PEG-functionalized lipids used, $R_G = 1.0$ nm.

Figure 2 shows representative force–distance profiles measured under different positive and negative externally applied electrochemical potentials, $\Delta U = U - U_{PZC}$, as defined in Fig. 1. The contact distance, $D = 0$, is defined as the distance measured between the gold electrode surface and the bare mica surface (with no PEG-functionalized lipid bilayer) in dry nitrogen under high load, with no fluid between the surfaces and no applied electrochemical potentials. Under these conditions, the Au surface is in direct contact with the mica surface.

Figure 2a and b shows the force–distance profiles measured for the PEG lipids with two different terminal chemical groups. Our results demonstrate that there are several differences between the force–distance profiles measured across bilayers with these two distinct polymer modifications, namely the $-\text{NH}_3^+$ and the $-\text{CH}_3$ termination. First, when the two surfaces are brought together (curves marked IN), polymer surfaces made from the different PEG-functionalized lipids approach to different characteristic “hard-wall” distances, T_{HW} , which is defined as the distance between the two surfaces at an applied force that is normalized by the surface radius of $F_{\text{max}}/R = 30$ mN/m (the maximum applied force).

The distance D_{HW} provides insight into the effective stiffness of the polymer chains. The PEG $-\text{NH}_3^+$ terminated surfaces can be compressed to hard wall distances ranging from 10 to 12.5 nm, while the PEG- CH_3 terminated surfaces can approach to hard-wall distances ranging from 7 to 9 nm at an applied F/R of 30 mN/m. Figure 3 indicates that the approach curves can be well described using a linear superposition of a polymer

mushroom repulsion [23,25], a steric hydration repulsion term [30], electric double layer interactions $F_{\text{EDL}}(D)$ (for details see [21]) and Van der Waals forces acting between the two surfaces:

$$\frac{F(D)}{R} = -\frac{A_H}{6D^2} + 72\pi k_B T \Gamma e^{\frac{(D-T_{\text{BL}})}{R_F}} - 4\pi\gamma H_\gamma e^{\frac{(D-T_{\text{HW}})}{D_H}} + \frac{F_{\text{EDL}}(D)}{R} \quad [\text{N/m}] \quad (1)$$

where R_F is the Flory radius, $D_H = 1$ nm is the characteristic decay length of the hydration repulsion [30], k_B is Boltzmann’s constant, T is the absolute temperature, $A_H = 2.5 \times 10^{-20}$ J/m² is the effective Hamaker constant, R is the mean radius of the crossed cylinder surfaces and $\Gamma = 2.1 \times 10^{16}$ molecules/m² is the surface concentration of the polymer mushrooms. The terms T_{BL} and T_{HW} are present to shift the plane of origin of mushroom and polymer dehydration forces to the PEG-functionalized bilayer surface. T_{HW} is found to be consistently further out than T_{BL} between 8 and 15 Å, representing an additional contribution to the measured distance that corresponds to the size of the compressed PEG chains. The data fits well with a Flory radius of $R_F = 3.3$ – 3.5 nm, indicating a good solvent situation with an R_F close to the expected value of 3.6 nm. Van der Waals interactions only weakly contribute to the overall measured interaction forces, and are overpowered by hydration and polymer mushroom interactions. The strength of electric double layer interactions depends on the applied electrochemical potential, but electric double layer interactions were also observed to be dominated by the polymer steric repulsions for these experimental conditions.

The third term in Equation (1) above accounts for hydrophobic (attractive) or steric-hydration (repulsive) interactions in water, both of which have been observed to have the same decay length of $D_H = 1$ nm and pre-exponential factor [30]. The value for the interfacial tension, $\gamma = 50$ mJ/m², is a reference value and chosen for comparison with previous work on hydrophobic and hydrophilic interfaces [30]. The Hydra parameter, H_γ , is a non-dimensional parameter that has a value $H_\gamma = 1$ for fully hydrophobic surfaces, $H_\gamma = 0$ for negligible contribution from hydrophobicity or hydrophilicity, and $H_\gamma < 0$ for hydrophilic surfaces, with larger negative values corresponding to increased affinity of water and hydrated ions at surfaces. In this work, $H_\gamma < 0$ as described below, resulting in repulsive hydration interactions arising from osmotic repulsions upon compressing the hydrated polymer chains and ions within the gap.

R_F , H_γ , and D_H were fitted as free variables, with consistent D_H values close to 1 nm for both polymer modifications. Figure 3 demonstrates that the theoretical form of Equation (1) is effective at describing the measured force–distance profiles. H_γ gives values of -0.05 for the PEG- CH_3 and -0.23 for the PEG $-\text{NH}_3^+$ case, respectively. This parameter is useful to gauge the binding affinity of ions and water at interfaces, with typical values for molecularly smooth hydrophilic surfaces ranging from -0.05 to -0.5 [21]. Interestingly, the larger value for H_γ for the $-\text{NH}_3^+$ head group reveals an increased repulsive energy needed to squeeze out hydrated ions and water molecules from the confined polymer [31]. PEG is well known for its ion and water retaining

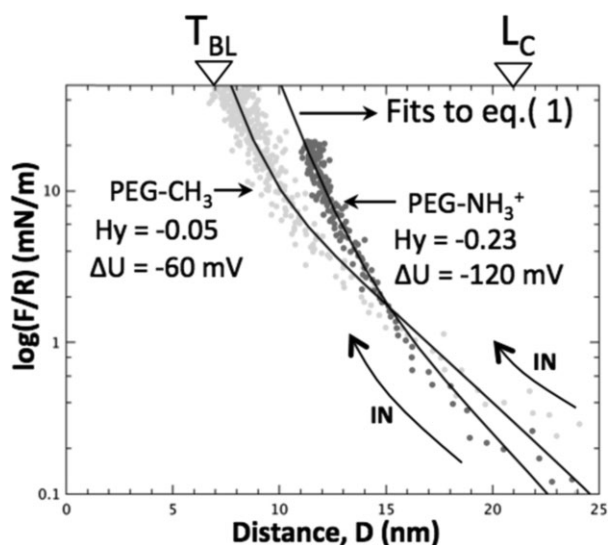


Figure 3. Force–distance profiles measured at $\Delta U = -60$ mV and $\Delta U = -120$ mV during approach for PEG- CH_3 (green) and PEG $-\text{NH}_3^+$, respectively and fits for both profiles to Equation (1)

properties [1]. This is not an unexpected result, as the positive charge of the $-\text{NH}_3^+$ functionality needs to be counterbalanced by an increased number of anions and their associated hydration shells. The H_y value for the PEG- CH_3 on the other hand is considerably smaller, indicating a decreased affinity of water and ions at the polymer-metal interface.

Figure 2a and b reveal that the resulting adhesion forces also exhibit large variations between the PEG- NH_3^+ and PEG- CH_3 containing bilayers. In particular, the adhesive forces have a strong potential dependence for the PEG- NH_3^+ case, while adhesion forces for the PEG- CH_3 case depend only weakly on the applied electrochemical potentials. Notably, while the repulsive forces measured on approach demonstrate that contacts of the metal electrode with the PEG- NH_3^+ terminated lipid bilayer surfaces are more heavily hydrated than for the PEG- CH_3 bilayers, the adhesion forces measured upon separation of the two surfaces are much higher in magnitude for the PEG- NH_3^+ bilayers than for the PEG- CH_3 bilayers. Further, this adhesion changes by a factor of up to 4 for the case of the PEG- NH_3^+ bilayers, depending on the electrochemical potentials, ΔU , that are applied to the gold surface. These changes in adhesion force are primarily due to the specific interaction of $-\text{NH}_3^+$ with the gold electrode surfaces, including the cases where gold oxide is present on the electrode surfaces at high anodic potentials, where $\Delta U > U_{\text{OX}}$.

Specific interactions are also directly reflected in the shape of the force-distance profiles plotted in Fig. 2a and b. The force profiles recorded during separation clearly show that the adhesive bindings do not break at distances D_{HW} where the hard wall is located. The adhesive bindings were instead observed to break at larger distances, denoted D_{jump} , where D_{jump} was observed to span a range of distances up to, but not further than, the full contour length L_C (indicated in the force-distance profiles) of the PEG-polymer tethers. This phenomenon has been well documented, and is typically known as a polymer bridging interaction [32]. These polymer-bridging interactions are indicative of two surfaces that are adhering through a polymer tether that is strongly attached to both interacting surfaces at different points in the polymer chain.

Figure 2c shows the potential dependence of the experimental adhesion forces F_{ADH} , which is defined as the minimum in the force-distance plot measured during separation of the gold electrode and the PEG-functionalized bilayer surface. From this data, adhesion energies can be directly calculated using Derjaguin's approximation [23] $W_{\text{ADH}} = F_{\text{ADH}}(D_{\text{jump}})/(2\pi R)$ [J/m^2]. Comparing the surface density of the polymer molecules, $\Gamma = 2.1 \times 10^{16}$ molecules/ m^2 , to the measured adhesion energies, $W_{\text{ADH}} = 1.1\text{--}4.7$ mJ/m^2 , allows the calculation of the adhesion energy per polymer molecule, which is plotted on the second y-axis in Fig. 2c.

Additionally, comparing the adhesion energies for $-\text{NH}_3^+$ and $-\text{CH}_3$ terminated PEG-molecules allows for quantification of the different contributions to the measured polymer chain-mediated adhesive interactions. For example, we can approximate what portion of the measured interaction energies are due to polymer chain and/or specific NH_3^+ terminal group interactions with the electrified gold surface. From these calculations, we determined that the $-\text{NH}_3^+$ /gold bond interaction energies range from 0.5 to

45 k_BT , depending on the applied electrochemical potential ΔU . For the CH_3 -terminated PEG, the results indicate that the sole contribution to the polymer-gold adhesive interaction is due to the interaction of PEG segments with the gold surface, that is, binding of the PEG polymer backbone to the gold surface, which yields interaction energies ranging from 6 to 12 k_BT per PEG, or 0.13–0.26 k_BT per polymer segment.

Further, the NH_3^+ terminated PEG-functionalized bilayers display minima in the measured adhesion energies around the potential of zero charge. Interestingly, this result suggests that the binding mechanism of the $-\text{NH}_3^+$ group is not exclusively based on electrostatic interactions between the gold surface and the positively charged $-\text{NH}_3^+$ functionality, although the electrostatic component of this interaction energy was the focus of previous work [25,33]. At applied electrochemical potentials $\Delta U < U_{\text{PZC}}$ the gold surface is negatively charged and may electrostatically attract the $-\text{NH}_3^+$ functionalities. On the other hand, at electrochemical potentials between the potential of zero charge and the gold oxidation potential, $U_{\text{PZC}} < \Delta U < U_{\text{OX}}$, the gold surface is positively charged and electrostatic interactions are expected to be repulsive. Comparing the adhesion values for the PEG- CH_3 and the PEG- NH_3^+ obtained at U_{PZC} , the interaction energy only amounts to 0.5 k_BT per $-\text{NH}_3^+$ /gold bond. Thus, the interactions of both of the PEG- CH_3 and the PEG- NH_3^+ polymers with gold surfaces at the U_{PZC} are dominated by the interactions of the PEG₄₅-backbone, resulting in similar adhesions for both cases. Notably, nitrate ions in the aqueous solutions are known to exhibit strong, specific interactions with gold surfaces at potentials around U_{PZC} [34], so the lack of specific NH_3^+ -gold interactions may be due to a protecting layer of nitrate ions strongly bound to the gold, effectively blocking the NH_3^+ groups.

Another subtlety arises at higher potentials, where the adhesion measured for the PEG- $(\text{NH}_3)^+$ rises again to values above 30–40 k_BT . For this potential range, nitrate ions will be electrochemically desorbed and become replaced by chemisorbed hydroxide ions [29]. In contrast to nitrates, adsorbed hydroxides may promote adhesion at higher potentials and in particular on the fully oxidized metal (above $\Delta U = 960$ mV) through condensation reactions. This effect is well known for metal-oxide surfaces, where adsorbed hydroxides considerably increase reaction kinetics for chemisorption of self-assembled monolayers [35–37]. In general, high adhesion energies and the observed bridging forces agree well with theoretical studies predicting strong specific interaction energies of amine functionalities with gold surfaces, in the range of 40 k_BT for one single- $-\text{NH}_3^+$ /gold bond [38]. Hence, the specific $-\text{NH}_3^+$ /gold interaction is much stronger than the non-specific interactions, such as Coulombic (typically 5–10 k_BT [23]) or Van der Waals interactions, at the polymer/metal surfaces.

Notably, the formation of specific bonds between the protonated $-\text{NH}_3^+$ functionalities and positive gold surfaces requires that repulsive electrostatic energy barriers are overcome if the positive chemical group approaches the positive electrode surface. The energy penalty associated with these electrostatic barriers would be eliminated if the amine functionalities become deprotonated when confined close to the positive electrode surface. Alternatively, confinement is known to lower

activation barriers for ion-transfer reactions, for instance for silica dissolution in confinement [19]. In any case, theoretical calculations suggest that the specific amine/gold bond is ultimately uncharged after forming [38]. These observations suggest, that the adhesion forces at positive potentials may strongly depend on contact times and maximum compressive loads (preloads). A detailed investigation of the time effects and prolonged contact times up to several hours is beyond the scope of this work, yet may have a significant influence on the measured adhesive forces [39].

In summary, we conclude that the adhesive minimum reflects a very delicate balance between ion-adsorption, backbone adsorption and $-\text{NH}_3^+$ adsorption energies and kinetics. Also, it is well known that the introduction of specific functionalities can be an effective strategy for promoting adhesion between metals and polymeric materials, yet the effects of these specific functionalities for example, on corrosion rates may be much more complex than previously expected [10,15]. As demonstrated in this work, introducing hydrophilic functional groups also leads to a much-increased water and ion content at an electrified polymer|metal interface. Thus, the design of adhesion-promoting polymers must be delicately balanced with optimizing the chemical structures of polymers that provide a significant retardation of corrosion reactions.

4 Conclusions

Figure 4 summarized our main results and the measured and distinguished interaction forces and energies. (1a in Fig. 4) The increased hydration repulsion measured in our experiments revealed that $-\text{NH}_3^+$ functionalization of the terminal end-group of PEG-molecules leads to an increased water and ion content at electrified $\text{PEG}_{45} - \text{NH}_3^+$ /gold interfaces compared to (1b in Fig. 4) PEG-CH_3 /gold interfaces.

We found that PEG-CH_3 polymers exhibit weak binding energies to the electrified gold surface ranging from 6 to $12 k_B T$ per PEG polymer, or about $0.13\text{--}0.26 k_B T$ per individual PEG segment. The measured range of the adhesive forces suggests that these interactions are due to weak Van der Waals interactions of the polymer backbone with the gold surface. This binding does not involve a charge-charge interaction, is non-specific and hence depends only weakly on the applied electrochemical potential.

We also showed that $-\text{NH}_3^+$ functionalities exhibit a strongly potential dependent, yet specific, binding interaction to gold surfaces leading to considerable bridging forces (panel 2 in Fig. 4) ranging from 0.5 to $45 k_B T$ per $-\text{NH}_3^+$ /gold bond, with a pronounced minimum around the potential of zero charge U_{PZC} . The strong binding energies compare well with recent simulation studies and indicate a weak covalent bond between gold and $-\text{NH}_3^+$. The minimum binding energy observed near U_{PZC} results from the complex interplay between hydration, specific ion adsorption to the gold surface, and the specific functional groups at the electrified polymer|metal interfaces. Extended time effects are also expected to play important role, and are currently under further investigation.

In summary, using an EC-SFA provides the possibility to unravel the delicate balance between polymer-backbone and polymer-functionalization, competitive specific ion and water adsorption at the interface and the applied electrochemical potential. We used this approach to quantify the influence on adhesion and stability of a polymeric and specific bonding at an electrified interface. Our approach may provide an effective technique to elaborate the effects of specific polymer modification in both technical and medical applications, where a desired binding interaction between metal, or metal oxides and polymer materials is needed for an optimized performance of composite materials. Our systematic approach provides the possibility to optimize technical systems for low and for high adhesion at given electrochemical potentials.

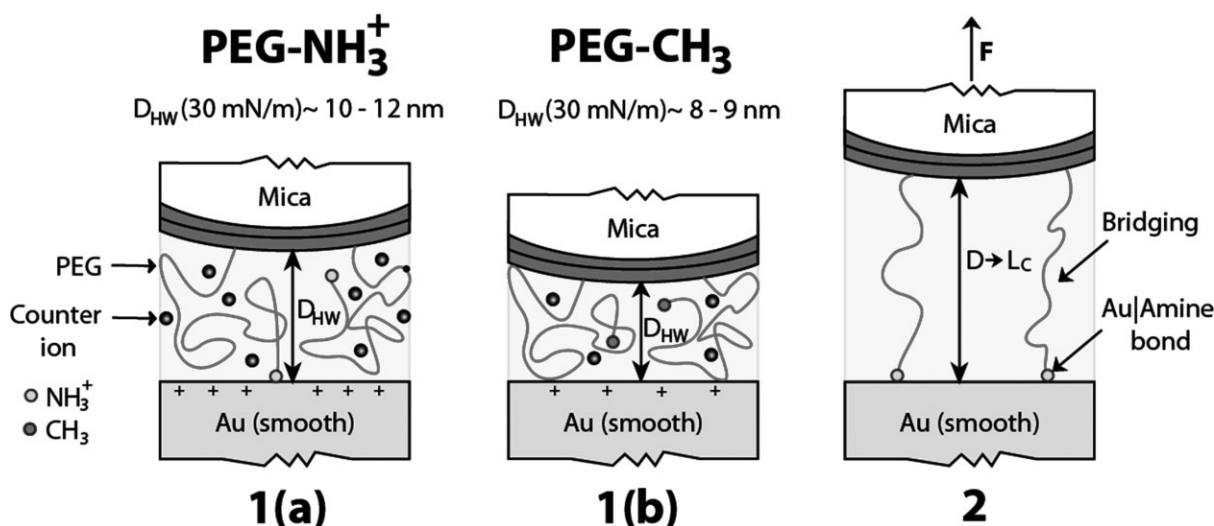


Figure 4. Schematic of the origins of the measured interaction forces. 1(a) shows the increased hard wall distances D_{HW} measured at $F = 30 \text{ mN/m}$ for $\text{PEG} - \text{NH}_3^+$ /gold interfaces as compared to the PEG-CH_3 bilayers, which is due to an increased ion and water concentration at the $\text{PEG} - \text{NH}_3^+$ interface. As depicted in 1(b), PEG-CH_3 /gold interfaces exhibit a decreased D_{HW} , which is related to less strongly bound hydration layer within the non-functionalized PEG. In (2) a schematic depicts how bridging forces can lead to an increased distance from which the surfaces jump apart

Acknowledgments: M.V. acknowledges financial support through a Marie Curie International Outgoing Fellowship within the 7th European Community Framework Program under Award No. IOF-253079.

T.U. acknowledges funding through the International Max Planck Research School for Surface and Interface Engineering in Advanced Materials (IMPRS-SurMat).

This research was supported by the Department of Energy, Office of Basic Energy Sciences, Division of Materials Sciences and Engineering, under Award DE-FG02-87ER-45331 (development of the SFA and electrochemical attachment, and the normal, adhesion and lateral, friction force measurements) and the U.S. National Science Foundation under Grant No. CHE-1059108.

5 References

- [1] T. L. Kuhl, D. E. Leckband, D. D. Lasic, J. N. Israelachvili, *Biophys. J.* **1994**, *66*, 1479.
- [2] A. E. Nel, L. Madler, D. Velegol, T. Xia, E. M. V. Hoek, P. Somasundaran, F. Klaessig, V. Castranova, M. Thompson, *Nat. Mat.* **2009**, *8*, 543.
- [3] A. Verma, F. Stellacci, *Small* **2010**, *6*, 12.
- [4] A. Lesniewicz, L. Gackiewicz, W. Zyrnicki, *Int. Biodeterior. Biodegrad.* **2010**, *64*, 81.
- [5] C. H. Li, K. Jordens, G. L. Wilkes, *Wear* **2000**, *242*, 152.
- [6] Y. Takahashi, M. Iijima, K. Inagawa, A. Itoh, *J. Vac. Sci. Tech. A* **1987**, *5*, 2253.
- [7] K. Hoffmann, M. Stratmann, *Corr. Sci.* **1993**, *34*, 1625.
- [8] M. Stratmann, R. Feser, A. Leng, *Electrochim. Acta* **1994**, *39*, 1207.
- [9] M. Stratmann, H. Streckel, *Mater. Corros.* **1992**, *43*, 316.
- [10] R. Feser, M. Stratmann, *Mater. Corros.* **1991**, *42*, 187.
- [11] M. Stratmann, H. Streckel, R. Feser, *Corr. Sci.* **1991**, *32*, 467–4470.
- [12] R. Posner, T. Titz, K. Wapner, M. Stratmann, G. Grundmeier, *Electrochim. Acta* **2009**, *54*, 900.
- [13] R. Posner, K. Wapner, M. Stratmann, G. Grundmeier, *Electrochim. Acta* **2009**, *54*, 891.
- [14] M. Stratmann, M. Wolpers, H. Streckel, R. Feser, *Phys. Chem. Chem. Phys.* **1991**, *95*, 1365.
- [15] M. Stratmann, *Adv. Mater.* **1990**, *2*, 191.
- [16] T. R. Khan, A. Erbe, M. Auinger, F. Marlow, M. Rohwerder, *Sci. Tech. Adv. Mater.* **2011**, *12*, 9.
- [17] M. Rohwerder, S. Isik-Uppenkamp, C. A. Amarnath, *Electrochim. Acta* **2011**, *56*, 1889.
- [18] J. N. Israelachvili, Y. Min, M. Akbulut, A. Alig, G. Carver, W. Greene, K. Kristiansen, E. Meyer, N. Pesika, K. Rosenberg, H. Zeng, *Rep. Prog. Phys.* **2010**, *73*.
- [19] K. Kristiansen, M. Valtiner, G. W. Greene, J. R. Boles, J. N. Israelachvili, *Geochim. Cosmochim. Acta* **2011**, *75*, 6882.
- [20] M. Valtiner, K. Kristiansen, G. W. Greene, J. N. Israelachvili, *Adv. Mater.* **2011**, *23*, 2294.
- [21] M. Valtiner, X. Banquy, K. Kristiansen, G. W. Greene, J. N. Israelachvili, *Langmuir* **2012**, *28*, 13080.
- [22] S. H. Kim, *J. Phys. Chem.* **1973**, *77*, 2787.
- [23] J. N. Israelachvili, *Intermolecular and Surface Forces*, 3rd Ed., Academic Press, Burlington, MA **2011**.
- [24] J. N. Israelachvili, *J. Coll. Interf. Sci.* **1973**, *44*, 259.
- [25] S. H. Donaldson, M. Valtiner, M. A. Gebbie, J. Harada, J. N. Israelachvili, *Soft Matter* **2013**, *9*, 5231.
- [26] L. Chai, J. Klein, *Langmuir* **2007**, *23*, 7777.
- [27] S. Garcia-Manyes, L. Redondo-Morata, G. Oncins, F. Sanz, *J. Am. Chem. Soc.* **2010**, *132*, 12874.
- [28] K. El. Kirat, S. Morandat, Y. F. Dufrene, *Biochim. Biophys. Acta Biomembr.* **2010**, *1798*, 750.
- [29] B. E. Conway, *Prog. Surf. Sci.* **1995**, *49*, 331.
- [30] S. H. Donaldson, S. Das, M. A. Gebbie, M. Rapp, L. C. Jones, Y. Roiter, P. H. Koenig, Y. Gizaw, J. N. Israelachvili, *ACS Nano* **2013**, *7*, 10094.
- [31] R. M. Espinosa-Marzal, R. M. Bielecki, N. D. Spencer, *Soft Matter* **2013**, *9*, 10572.
- [32] N. W. Moore, T. L. Kuhl, *Biophys. J.* **2006**, *91*, 1675.
- [33] D. V. Leff, L. Brandt, J. R. Heath, *Langmuir* **1996**, *12*, 4723.
- [34] N. S. Marinkovic, J. J. Calvente, A. Kloss, Z. Kovacova, W. R. Fawcett, *J. Electroanal. Chem.* **1999**, *467*, 325.
- [35] M. Chockalingam, N. Darwish, G. Le Saux, J. J. Gooding, *Langmuir* **2011**, *27*, 2545.
- [36] D. Snihirova, L. Liphardt, G. Grundmeier, F. Montemor, *J. Solid State Electrochem.* **2013**, *17*, 2183.
- [37] W. P. Vellinga, G. Eising, F. M. de Wit, J. M. C. Mol, H. Terryn, J. H. W. de Wit, J. T. M. de Hosson, *Mater. Sci. Eng. A* **2010**, *527*, 5637.
- [38] S. Goel, K. A. Velizhanin, A. Piryatinski, S. Tretiak, S. A. Ivanov, *J. Phys. Chem. Lett.* **2010**, *1*, 927.
- [39] D. W. Lee, C. Lim, J. N. Israelachvili, D. S. Hwang, *Langmuir* **2013**, *29*, 14222.

(Received: December 19, 2013)

W7581

(Accepted: January 5, 2014)